Waterborne GPR survey for estimating bottom-sediment variability: A survey on the Po River, Turin, Italy

GEOPHYSICS, VOL. 74, NO. 4 (JULY-AUGUST 2009); P. B95–B102, 8 FIGS., 4 TABLES.
10.1190/1.3119262

Case History

Waterborne GPR survey for estimating bottom-sediment variability: A survey on the Po River, Turin, Italy

Luigi Sambuelli[1], Corrado Calzoni[1], and Manuele Pesenti[1]

ABSTRACT

We conducted an integrated geophysical survey on a stretch of the river Po in order to check the GPR ability to discriminate the variability of riverbed sediments through an analysis of the bottom reflection amplitudes. We conducted continuous profiles with a 200-MHz GPR system and a handheld broadband EM sensor. A conductivity meter and a TDR provided punctual measurements of water conductivity, permittivity, and temperature. The processing and interpretation of the GEM-2 and GPR data were enhanced by reciprocal results and by integration with the punctual measurements of the EM properties of the water. We used a processing flow that improved the radargram images and preserved the amplitude ratios among the different profiles and the frequency content at the bottom reflection signal. We derived the water attenuation coefficient both from the punctual measurements using the Maxwell formulas and from the interpretation of the GPR data, finding an optimal matching between the two values. The GPR measurements provided maps of the bathymetry and of the bottom reflection amplitude. The high reflectivity of the riverbed, derived from the GPR interpretation, agreed with the results of the direct sampling campaign that followed the geophysical survey. The variability of the bottom-reflection-amplitudes map, which was not confirmed by the direct sampling, could also have been caused by scattering phenomena due to the riverbed clasts which are dimensionally comparable to the wavelength of the radar pulse.

INTRODUCTION

This work deals with acquiring, processing, and interpreting waterborne ground-penetrating-radar (GPR) data to survey bathymetry changes and discriminate between riverbed sediments. We collected GPR data on the Po River (Turin, Italy) in autumn 2005. We also acquired low-frequency electromagnetic, time-domain reflectometer (TDR), conductivity, and temperature measurements during the same campaign (Sambuelli et al., 2007). Months later (April 2006), we sampled the river bottom.

Monitoring river erosion and understanding the connection between surface water and underground water are critical environmental issues. Interest applying GPR to shallow-water environments is growing, as shown by several publications related to this topic. Early applications of GPR in water environments (Annan and Davis, 1977; Kovacs, 1978) were conducted in low-conductivity media, such as melting water in arctic areas. A high penetration depth can be achieved in such low-conductivity water: examples exist of subbottom penetration in water depths exceeding 25 m (Delaney et al., 1992). Other works attempt to obtain bathymetric maps of ice-covered lakes (Moorman et al., 2001; Schwamborn et al., 2002) and reservoirs (Arcone et al., 1992; Hunter et al., 2003; Best et al., 2005). Improvements in GPR technology now allow good penetration in conductive water (Arcone et al., 2006a). A system whose emitted power is enhanced by a factor of 1000, designed for acquisitions in shallow seawater (Abramov et al., 2004), has penetrated 1–2 m in sediments saturated by saltwater.

Thanks to its flexibility and potential, GPR is a reliable tool for assessing bridge scour (Davidson et al., 1995; Olimpio, 2000; Webb et al., 2000; Park et al., 2004), monitoring stream discharge (Haeni et al., 2000; Melcher et al., 2002; Cheng et al., 2004; Costa et al., 2006), studying sedimentology of bottom deposits (Buynevich and Fitzgerald, 2003; Fuchs et al., 2004; Shields et al., 2004), mapping bathymetry (Moorman and Michel, 1997; Powers et al., 1999; Jol and Albrecht, 2004), and finding submerged objects such as lumber (Jol and Albrecht, 2004). Many authors agree that GPR could provide complementary information to seismic methods, especially in very shallow water where reverberation can prevent the interpretation of subbottom reflectors (Arcone et al., 2006b) or when gas in the sediment prevents seismic signal penetration (Delaney et al., 1992; Mellett, 1995; Powers et al., 1999; Schwamborn et al., 2002).

The versatility of GPR is also the result of the flexibility of survey setups. Case histories report the use of antennas directly coupled to

Manuscript received by the Editor 22 April 2008; revised manuscript received 12 January 2009; published online 12 May 2009.
[1]Politecnico di Torino, Dipartimento di Ingegneria del Territorio, dell'Ambiente e delle Geotecnologie, Torino, Italy. E-mail: luigi.sambuelli@polito.it; corrado.calzoni@polito.it; manuele.pesenti@polito.it.

water from the surface (Sellmann et al., 1992; Mellett, 1995), prototypes of submerged antennas (Meyers and Smith, 1998; Tóth, 2004), noncontact systems such as helicopter mounts (Melcher et al., 2002) or hanging ropes (Costa et al., 2000; Haeni et al., 2000; Cheng et al., 2004), and antennas mounted on the bottom of nonmetallic boats (Jol and Albrecht, 2004; Park et al., 2004; Porsani et al., 2004; Bradford et al., 2005).

The potential of GPR to detect the composition of a riverbed has been mentioned in early studies. Ulriksen (1982) suggests that fine sediments can be identified from strong and smooth reflectors and moraine can be identified from speckled and weak signals; boulders may produce hyperbolic diffractions. The same qualitative approach to the analysis of basin-bottom characteristics has been tested positively by others (Beres and Haeni, 1991; Powers et al., 1999). In particular, Dudley and Giffen (1999) find optimal agreement between GPR results and direct sampling of sediments. However, there seems to be little documentation concerning sediment discrimination through a quantitative analysis of amplitude. Our work aims to provide a methodology to perform an approximate characterization of river-bottom sediment by mapping the GPR amplitude of reflection (AOR).

The possibility of a quantitative analysis of bottom AOR derives from assumptions that the signal transmitted in the water is constant and the river water is homogeneous with respect to the EM field. We verified the first assumption through preliminary tests, checking the constancy of the main bang (the first reflection event in a radargram acquired with a near-zero-offset bistatic antenna) obtained from the water's surface. The second assumption is particularly true in shallow rivers where there is no thermocline and therefore no reflectors before the riverbed (Bradford, 2007). We based the corrections of the radargrams for geometric spreading and water attenuation on this latter assumption.

Our methodology is grounded on the hypothesis that after these corrections have been made, the AOR from the riverbed sediments depends mainly on the type of sediments and is not correlated to the water depth. However, at least another two geometric factors may affect AOR: slope and the rugosity of the river bottom. Regarding the presence of a dipping reflector, we calculated the gradient of the bathymetry map and verified that more than 95% of the surveyed area has a slope angle below 4°. We hypothesized that the rugosity of the river bottom was negligible compared to the wavelength. This hypothesis, however, was not confirmed by the direct sampling campaign.

Even though we could not estimate the real reflection coefficient because we did not have information about the amplitude of the signal that entered the water, we considered the possibility of correlating the AOR variability to the variability in the riverbed sediments.

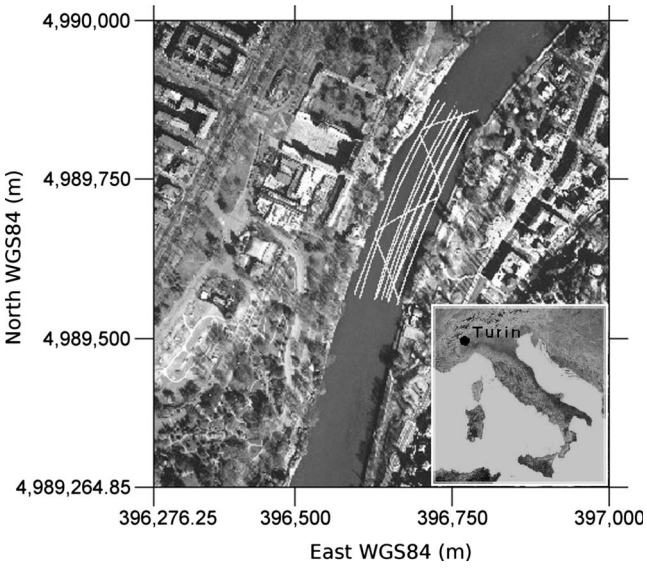

Figure 1. Location of the 10 processed GPR profiles acquired on the Po River in Turin, Italy. The river flows from south to north. Profile 1 is near the west bank, and profile 9 is near the east bank. Profile 10 is the crooked profile.

DATA ACQUISITION

To test our methodology, we chose a 300-m-long stretch of the Po River in Turin, northwest Italy. We performed a geophysical survey in autumn 2005 and then a bottom sampling survey in spring 2006, choosing the sampling points according to the results of the analysis performed on the geophysical data.

We conducted the first survey in two steps. First, we collected continuous data with an IDS K2 GPR and a Geophex GEM-2 handheld broadband EM sensor. Immediately after the continuous acquisitions, we collected spot measurements of water permittivity with a Tektronic 1502c time-domain reflectometer (TDR) and measured water conductivity and temperature with a ProfiLine-197 conductivity meter. We referred both acquisitions to the UTM WGS84 absolute reference system with a real-time kinematic (RTK) global positioning system (GPS). For additional details about boat positioning and tracking, refer to Sambuelli et al. (2007).

A pulsed-radar IDS K2 GPR with a TR200 IDS unit, a nominal 200-MHz central-frequency bistatic antenna, was placed on the flat bottom of a fiberglass boat. We tested the antenna in the air with a plane reflector in the far field and obtained an effective central frequency of 250 MHz. We opted to place the antenna in the boat and excluded other possibilities. We avoided noncontact methods because hanging the antenna over the water's surface would have widened the emission cone and multiple patterns in the air, minimizing horizontal resolution and introducing noise in the radargrams. We also excluded a system with a submerged towed antenna because the cable could have been snagged by submerged objects such as tree trunks or WWII unexploded ordnance (UXO). Moreover, placing the antenna on the water's surface allows bathymetry estimation.

We acquired 10 profiles, nine parallel to the shorelines and one along a crooked line intersecting the others along four different segments at an approximate angle of 45° (Figure 1). All GPR profiles were acquired using the same configuration, with the acquisition parameters reported in Table 1.

Physical and chemical properties of water, such as temperature and salinity, influence water conductivity and permittivity, which in turn affect the velocity and attenuation of a radar pulse. For example, the vertical gradients of these properties could influence the velocity of the radar waves (Ellison et al., 1996) and consequently bathymetry accuracy. To provide information on the variability of the water properties in the investigated area and to check the vertical gradients, we measured temperature, conductivity, and permittivity from the water's surface to a depth of 2 m in 0.5-m steps (Table 2). We took these measurements at 14 points distributed spatially along three lines parallel to the axis of the river — one line near the west

bank, one near the east bank, and the other approximately coincident with the river's axis — with about five points per line.

The bottom sampling survey was performed in April 2006, when the geophysical survey was interpreted. No flood events occurred between the surveys. During this 2006 survey, we selected 12 points to scan the bathymetry range and to sample different reflectivity areas. The bottom sampling results are reported in Table 3.

DATA PROCESSING

We used the conductivity meter and TDR to measure the Po River water and obtained the values of the EM properties reported in Table 2 for different water depths. This analysis shows the homogeneity of the water flowing in the surveyed area and the lack of significant vertical gradient. We then calculated the average and standard deviation values (Table 2) of the conductivity σ, permittivity ε_r, and temperature T. With the Maxwell formulas, we calculated attenuation α, propagation factor β, velocity V, and wavelength λ of a pulse with a dominant frequency f of 200 MHz in the water with the aforementioned average values of the EM parameters and a relative magnetic permeability μ_r of one. The results are shown in Table 4.

Before processing the GPR data, we windowed the main bangs of all traces and assessed the repeatability of the signal. Figure 2 shows all 8545 raw main bangs of the 10 profiles acquired in the survey. All signals are very similar, and overlapping occurs in several points. Similar results are very unusual in terrain acquisitions; but in water applications, it is easy to ensure a constant coupling between the antenna, boat, and water. The water impedance usually remains homogeneous along a survey area.

Data processing preserved, as much as possible, the amplitude ratios among different traces and profiles and the frequency content of the reflections from the river bottom. Processing followed these steps.

1) Correct zero time — remove the time delay added to the acquisition before the main bang to obtain the zero time coinciding with the beginning of the trace.
2) Dewow — remove the very-low-frequency components from all traces, present in the signal because the acquisitions were performed without a filter.
3) Cut time — the maximum two-way time of the bottom reflection was always less than 180 ns. The time cut reduced the trace length from 400 ns to 200 ns.
4) Background removal — apply a high-pass horizontal filter to the profiles to remove a horizontally coherent component from ringing at 200 MHz. (Had we not applied background removal, the next two steps — divergence compensation and gain function — would have amplified the ringing.)
5) Compensate for divergence — recover the geometric spreading.
6) Gain function —recover the intrinsic attenuation with the attenuation coefficient given by the regression to obtain the AOR of the river-bottom sediments.
7) Time and amplitude reflection picking — pick the times and AOR with the UTM coordinates of each point to produce the final bathymetric and AOR maps.

Table 1. Acquisition parameters of the IDS K2 GPR.

Acquisition parameter	
Antenna nominal central frequency	200 MHz
Acquisition rate	6 traces/s
Mean distance between trace	0.3 m
Gain	No
Samples per trace	2048
Recording time	400 ns
GPS logging frequency	1 Hz

Table 2. Punctual measurement results: mean and standard deviation, evaluated on 14 points, of the water conductivity, temperature, and permittivity at different depths.

	Conductivity (mS/m)		Temperature (°C)		Permittivity (−)	
Water depth (m)	Mean	Std	Mean	Std	Mean	Std
0	36.8	0.64	13.3	0.12	85.1	3.35
0.5	36.8	0.48	13.3	0.06	84.1	3.22
1	36.7	0.44	13.2	0.06	85.0	3.21
1.5	36.8	0.42	13.2	0.06	83.3	2.81
2	36.7	0.07	13.3	0.07	—	—
All depths	36.7	0.46	13.3	0.08	84.4	3.17

Details on background-removal method, step 4

The background-removal subtracts the average trace of each profile from each trace. In this way, the reflection events are averaged and part of the information is lost. The more horizontal the reflective interfaces, the more their weight increases on average and the more information is lost. To respect the information content more, we could subtract a reference trace, corresponding to the deepest zone of the profile, from each profile to remove the ringing and not disturb the AOR for most of the data.

We tested both procedures; because of the nonhorizontality of the river bottom, the results were quite similar. We then selected the background-removal method because the ringing was not completely in-phase throughout each profile and the averaging, in the background removal procedure, could account for this better. However, if the ringing were in-phase, subtracting a reference trace would be more effective.

Details on divergence compensation, step 5

We could not estimate the radiation pattern of the antennas, so it was not taken into account in this correction. Divergence compensation acts on each trace, recovering the geometric divergence losses. We multiplied the amplitudes of each sample of each trace by its two-way time multiplied by the pulse velocity in the water, assuming we

were in the Fraunhofer region with spherical loss. This assumption implicitly means that the downgoing wavefront is spherical and can be approximated locally with a plane wave. The wave then impinges on a flat surface and the upgoing wavefront is planar. This is equivalent to hypothesizing an image source symmetrical to the real source with respect to the reflecting surface.

Details on gain function, step 6

After applying the divergence compensation, we picked the positive maximal AOR values of the riverbed and the relative depths. To perform the picking operation quickly, we adopted the interpolated autopicking feature available in Sandmeier's Reflex-Win software. We isolated the reflection events by muting the amplitudes of the traces above and below the bottom reflection to guide the autopicking. Then we estimated the reflection depths with the two-way time using a water velocity value equal to 0.033 m/ns. A depth range of 1–3 m allowed us to consider, even in the shallowest condition, the reflection geometry as nearly vertical, the distance between the transmitter and receiver dipoles being 0.19 m. The autopicking failed at a limited number of locations where the water depth was greater than 3 m: we did not collect the amplitudes at these locations.

After checking input signal uniformity, water homogeneity, and nearly vertical reflection geometry, and after divergence compensation, the AOR should follow an exponential decay with respect to the water depth Z_w according to the equation

$$\frac{\mathrm{AOR}}{A_0} = e^{-\alpha \cdot 2 \cdot Z_w}, \tag{1}$$

where A_0 is the amplitude of the wave entering the water and $\alpha(\mathrm{m}^{-1})$ is the water attenuation coefficient. The spherical loss assumption, together with the Rayleigh scattering condition, would then imply that the difference in the AOR from the exponential trend should be given mainly by the difference of EM characteristics of the reflecting medium, that is, the bottom sediments.

Figure 3 shows all of the collected picked amplitudes versus twice the water depth together with the least-squares regression exponential, identified by the equation,

Table 3. Riverbed sampling results at each point with a brief description of the sampled sediments, the dimension of the maximum clast collected in the sampling point, its size parameter estimated with equation 4 for a wavelength of 0.16 m, the water depth, and the AOR corresponding to the sampling point.

Sampling points	Sample description	Maximum clast diameter (cm)	Maximum size parameter (−)	Water depth (m)	AOR (dB)
1	4 cobbles with a small amount of sandy silt	6	1.18	1.66	−13.8
2	4 cobbles with a small amount of sandy silt	6	1.18	1.16	−12.7
3	3 cobbles in a gravel matrix with silty sand	9	1.77	1.29	−19.2
4	1 cobble in a silt and gravel matrix	7	1.37	1.24	−7.37
5	Silt with sandy gravel	<1	0.20	1.42	−8.28
6	3 cobbles with sandy-silty gravel	8	1.57	1.61	−11.3
7	1 cobble in a sandy-gravelly silt	7	1.37	1.57	−15.1
8	2 cobbles with sandy-silty pit-run gravel	10	1.96	1.69	−12.7
9	1 cobble covered by silt	9	1.77	2.84	−13.4
10	2 cobbles with pit-run gravel (relatively abundant)	8	1.57	3.05	−10.5
11	Gravel with sand	<1	0.20	2.83	−7
12	2 cobbles in a gravel-silty sand matrix	6	1.18	2.68	−15.3

Table 4. Electromagnetic properties of the water estimated with the Maxwell formulas from conductivity and permittivity measurements.

ε_r (−)	σ (mS/m)	μ_r (−)	f (MHz)	α (m^{-1})	β (m^{-1})	V (m/ns)	λ (m)
84	36.8	1	200	0.756	38.4	0.033	0.16

$$\mathrm{AOR} = 11{,}540 \cdot e^{-0.743 \cdot 2 \cdot Z_w}. \quad (2)$$

The value of the attenuation coefficient, 0.743 m^{-1}, estimated from the regression of the AOR, differs by less than 2% from that estimated with the Maxwell relation, 0.756 m^{-1}.

RESULTS

Applying the processing flow to the raw data improved the radargrams. Figure 4 compares the radargram of profile 4 (the third from the west bank) before and after processing; both images are plotted with the same amplitude scale. All of the processed radargrams show sharp contrasts in the bottom reflections. This high reflectivity prevents an unambiguous identification of the reflections within the sediments.

We converted the bottom reflection times into the water depths by using the velocity of the radar waves in the water. We then gridded the results to obtain the bathymetric map shown in Figure 5. The water depth in the surveyed area increased from the east bank going toward the west bank, and almost all of the depths are included in the 1–3-m interval. The trend of the bathymetry agrees with the fluvial geomorphology. The river, flowing from south-southwest to northeast, has a slight curvature (Figure 1), and the flow has a higher velocity near the west bank where erosion occurs, which is more effective than near the east bank.

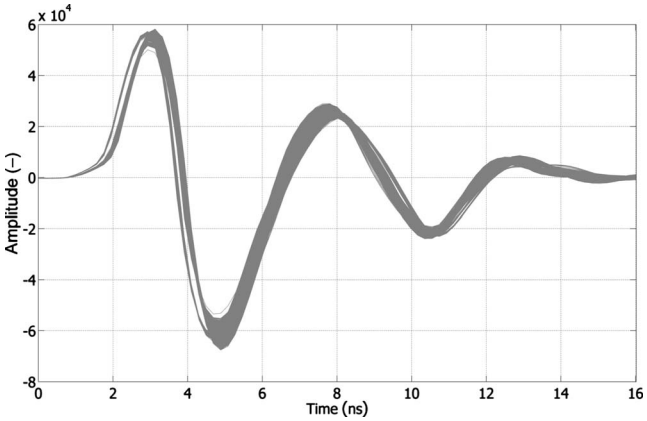

Figure 2. Main bang repeatability. The 8545 raw main bangs of the 10 acquired profiles are plotted. Plot overlapping is from the high similarity of the traces.

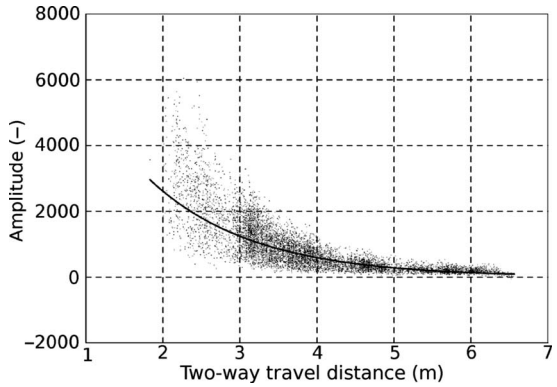

Figure 3. The continuous line represents the least-squares exponential regression (equation 2) on the 8059 amplitudes of reflection (black dots) picked after the divergence compensation versus the distance travelled by the radar pulse.

To map the bottom AOR, we converted all of the picked AOR values in decibels ($\mathrm{AOR}_{[dB]}$) according to

$$\mathrm{AOR}_{[db]} = 20 \cdot \log\left(\frac{\mathrm{AOR}}{\mathrm{AOR}_{max}}\right), \quad (3)$$

where AOR_{max} is the maximum bottom AOR measured in the surveyed area. Figure 6 shows the bottom AOR map expressed in decibels. This map shows only a relative homogeneity of the bottom sediments and is uncorrelated to the bathymetry map shown in Figure 5.

To help interpret the bottom AOR map, we graphed all 8958 amplitude values in the histogram in Figure 7. More than 75% of the area is characterized by values included in the −15 and −6 dB. We can assume that most of the points have a high AOR. Such a result agrees with the radargrams, where the penetration of the signal in the

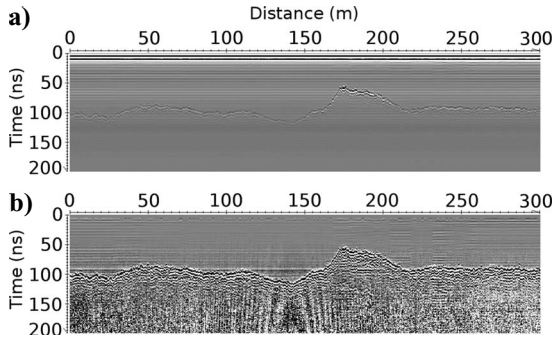

Figure 4. Comparison between (a) raw and (b) processed radargrams of profile 4, the third from the west bank. The images are plotted with the same amplitude scale.

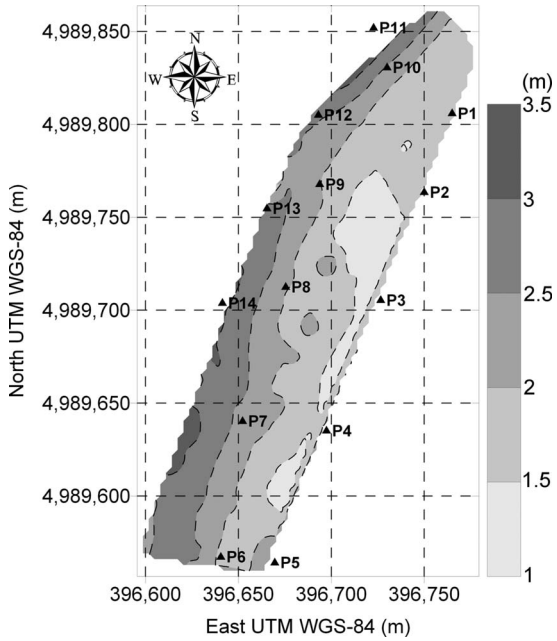

Figure 5. Bathymetric map of the surveyed stretch of the Po River, estimated with GPR two-way time and assuming a radar-wave velocity of 0.033 m/ns in the water.

sediments is very poor. Moreover, the sampling surveys revealed the relevant presence of coarse clasts in a sandy matrix, and these sediments have a higher reflectivity than homogeneous fine sediments (Powers et al., 1999; Shields et al., 2004). Finally, the GPR interpretation agrees with the EM survey response described in Sambuelli et al. (2007), where resistivity values compatible with saturated gravel and coarse clasts are reported. The agreement is greater in the widespread high reflectivity in the map than in a correspondence between high-reflectivity and high-resistivity areas.

The inhomogeneity of the map, with respect to the homogeneity of the direct sampling results, could be explained by two main hypotheses: (1) a heterogeneity of the sediments not detected by dredging and (2) a noncorrespondence of the reflector type to our previous hypothesis, particularly with reference to Rayleigh scattering. The first hypothesis can be confirmed by results in Sambuelli et al. (2007), where an incomplete uniformity of the bottom sediment conductivity is highlighted. The second hypothesis could be suggested by analyzing the ratio between the dominant pulse wavelength and the average pebble diameter.

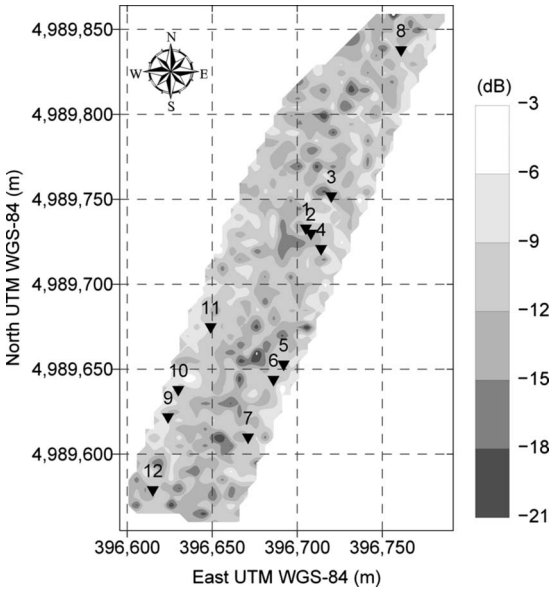

Figure 6. Contour map of the bottom amplitudes of reflection expressed in decibels. The 12 black triangles identify the direct sampling points.

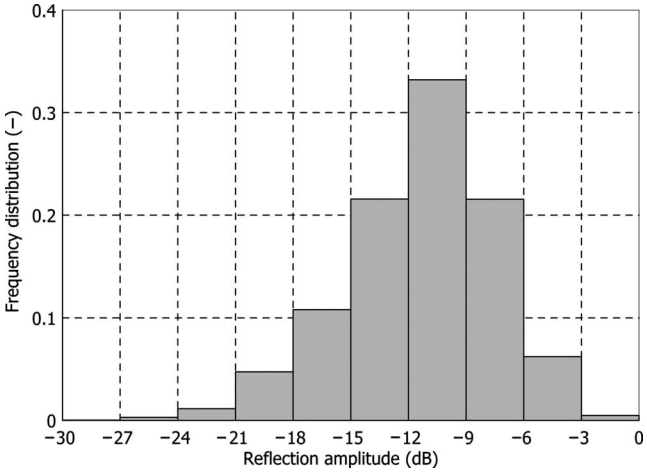

Figure 7. Frequency distribution of the bottom amplitudes of reflection after applying the processing flow. The histogram was computed from 8958 samples.

When dealing with scattering problems, it is usual to define a size factor x as

$$x = \frac{2 \cdot \pi \cdot r}{\lambda}, \tag{4}$$

where r is particle radius and λ is wavelength. The Rayleigh scattering condition requires $x \ll 1$. This condition allows us to consider the heterogeneous material as being homogeneous; when hit by a plane wave (providing a plane interface), it reflects a plane wave. To estimate the dominant wavelengths and to test the effectiveness of the procedure in maintaining the frequency content of the signals, we first extracted, with a tapered window, only the reflection event from each raw and processed trace and calculated the dominant frequency of the spectrum of each trace. The average dominant frequency of the reflected signals was 200 MHz in the raw and processed data. This result confirmed that processing did not affect the frequency content of the reflected signal. Despite coupling with a high-permittivity medium, a very small shift occurred with respect to the effective antenna frequency, toward the lower frequencies.

Then we calculated the dominant wavelengths with the GPR pulse velocity in the water and the dominant frequencies. We plotted the histogram of the dominant wavelengths of the processed reflected signals in Figure 8. The histogram clearly suggests that the dominant wavelength in the water is near 16 cm. This wavelength is about twice the average diameter of many of the sampled pebbles. Based on such a wavelength/particle size ratio, the hypothesis of a reflected plane wave is impossible, at least at a local scale. In fact, when $x \approx 1$, the Mie solution of Maxwell's equations better describes the scattering.

In Mie conditions, the radar cross section of the illuminated object is dependent on its dimension and on the signal wavelength. Consequently, the reflected amplitudes toward the receiver are like a random sum of backscattered diffuse signals rather than a plane wave (Kingsley and Quegan, 1992). Moreover, the Mie condition would prevent the use of a mixing rule approach to give a relation between the reflection coefficient and the permittivity of the sediments, the

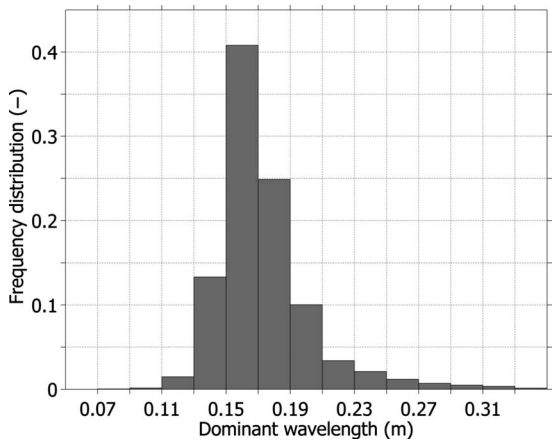

Figure 8. Frequency distribution of the dominant wavelengths estimated from the power spectra of the signal reflected by the river bottom. The histogram was computed from 7678 samples.

mixing rules being valid only in the Rayleigh condition (Sihvola and Alanen, 1991).

CONCLUSIONS

We have presented results related to GPR data derived from an integrated geophysical survey, where, contemporarily to the GPR measurements, we acquired low-induction-number EM multifrequency measurements (GEM-2). We also made some spot measurements of water permittivity, conductivity, and temperature and conducted a direct sampling survey. Our goal was to distinguish the riverbed sediments through a quantitative analysis of the river-bottom reflection amplitudes and conductivities.

As far as the quantitative analysis of the bottom reflections is concerned, we first checked the constancy of the signal that entered the water by checking the main bang repeatability. We then designed the data processing so that it did not significantly affect the frequency content of the signals and preserved the amplitude ratios among the different traces and profiles.

The processing and the interpretation of the GEM-2 and GPR data were enhanced by the reciprocal results and by integration with the spot measurements of the EM properties of the water. The spot permittivity and conductivity measurements allowed an estimation of the GPR pulse velocity, which we then used to obtain a bathymetry map. We used the bathymetry data obtained from the GPR for the transformation of the apparent conductivity data into sediment conductivity. We also calculated the attenuation factor, using the Maxwell formulas applied to the spot measurements. We used this value, which optimally matched the one estimated in our analysis of the GPR amplitudes, to correct the signal amplitudes and to obtain the AOR map.

However, we did not find an optimal agreement between GPR interpretation and direct sampling. Although direct sampling suggests an overall homogeneity of the river bottom, the AOR map shows areas with different values. The difference could be the result of scattering phenomena from pluricentimetric clasts and the sampling method. As far as the direct sampling is concerned, the Van Veen grab bucket did not provide detailed information on the sediments. A different sampling method that can collect a larger amount of coarse sediments without losing the finest should be recommended for geologic settings similar to this stretch of the Po River.

We did not find a one-to-one relationship between the AOR and the conductivity maps either. Agreement between the two maps and the direct sampling could only be found in a broad sense. The conductivity values of the river-bottom sediments are compatible with coarse saturated materials; the same holds for the high reflectivity of the river bottom. Both of these interpretations agree with the coarse clasts obtained from the direct sampling.

With respect to the field settings, the antenna placed on the flat bottom of a fiberglass boat was a good compromise between signal quality and an easy logistic configuration. However, the best solution is a purposely designed antenna with the dipole submerged in water to avoid power losses in the air and to limit the coupling effect between air and water. The optimum arrangement for a nonseismic river survey could be a multisensor boat that is RTK-tracked with a GPR, a low-frequency conductivity meter, electrical resistivity tomography (ERT) equipment with floating electrodes, and a device to acquire water permittivity, conductivity, and temperature data continuously.

ACKNOWLEDGMENTS

The authors thank the Reale Società Canottieri Cerea of Turin for logistic support, Alberto Godio for TDR measurements and fruitful discussions, Stefano Stocco for conductivity meter measurements, Alessandro Mottino for cooperating in the processing, Chiara Porporato for help in the GPS operations, and Hydrodata S.p.a. for sampling the bottom sediments. Finally, the authors thank the reviewers whose observations substantially improved the paper.

REFERENCES

Abramov, A. P., A. G. Vasiliev, V. V. Kopeikin, and P. A. Morozov, 2004, Underwater ground penetrating radar in archeological investigation below sea bottom: Proceedings of the 10th International Conference on Ground Penetrating Radar, 455–458.

Annan, A. P., and J. L. Davis, 1977, Impulse radar applied to ice thickness measurements and freshwater bathymetry: Report of Activities Part B, Geological Survey of Canada.

Arcone, S. A., E. F. J. Chacho, and A. J. Delaney, 1992, Short-pulse radar detection of groundwater in the Sagavanirktok River floodplain in early spring: Water Resources Research, **28**, 2925–2936.

Arcone, S. A., D. Finnegan, and J. E. Laatsch, 2006a, Bathymetric and subbottom surveying in shallow and conductive water: Proceedings of the 11th International Conference on Ground Penetrating Radar, on CD-ROM.

Arcone, S. A., D. C. Finnegan, and L. Liu, 2006b, Target interaction with stratigraphy beneath shallow, frozen lakes: Quarter-wave resonances within GPR profiles: Geophysics, **71**, no. 6, K119–K131.

Beres, M., and F. P. Haeni, 1991, Application of ground-penetrating-radar methods in hydrogeologic studies: Ground Water, **29**, 375–386.

Best, H., J. P. McNamara, and L. Liberty, 2005, Association of ice and river channel morphology determined using ground-penetrating radar in the Kuparuk River, Alaska: Arctic, Antarctic, and Alpine Research, **37**, 157–162.

Bradford, J. H., 2007, Advanced processing and acquisition methods to image within and beneath shallow water bodies with ground-penetrating-radar: 69th Conference & Exhibition, EAGE, Proceedings for Workshop on High Resolution Geophysics for Shallow Water.

Bradford, J. H., J. P. McNamara, W. Bowden, and M. N. Gooseff, 2005, Measuring thaw depth beneath peat-lined arctic streams using ground-penetrating radar: Hydrological Processes, **19**, 2689–2699.

Buynevich, I. V., and D. M. Fitzgerald, 2003, High-resolution subsurface (GPR) Imaging and sedimentology of coastal ponds, Maine, U. S. A.: Implications for Holocene back-barrier evolution: Journal of Sedimentary Research, **73**, 559–571.

Cheng, R. T., J. W. Gartner, R. R. J. Mason, J. E. Costa, W. J. Plant, K. R. Spicer, F. P. Haeni, N. B. Melcher, W. C. Keller, and K. Hayes, 2004, Evaluating a radar-based, non contact streamflow measurement system in the San Joaquin River at Vernalis, California: U. S. Geological Survey.

Costa, J. E., R. T. Cheng, F. P. Haeni, N. B. Melcher, K. R. Spicer, E. Hayes, K. Hayes, W. J. Plant, C. Teague, and D. Barrick, 2006, Use of radars to monitor stream discharge by noncontact methods: Water Resources Research, **42**, W07422.

Costa, J. E., K. R. Spicer, R. T. Cheng, F. P. Haeni, N. B. Melcher, E. M. Thurman, W. J. Plant, and W. C. Keller, 2000, Measuring stream discharge by non-contact methods: A proof-of-concept experiment: Geophysical Research Letters, **27**, 553–556.

Davidson, N. C., M. S. A. Hardy, and M. C. Forde, 1995, Bridge scour assessment by impulse radar: Institution of Electrical Engineers (IEE) Colloquium on Radar and Microwave Techniques for Non-Destructive Evalution, 8-1–8-8.

Delaney, A. J., P. V. Sellmann, and S. A. Arcone, 1992, Sub-bottom profiling: A comparison of short-pulse radar and acoustic data: Proceedings of the 4th International Conference on Ground Penetrating Radar, 149–157.

Dudley, R. W., and S. E. Giffen, 1999, Composition and distribution of streambed sediments in the Penobscot River, Maine: U. S. Geological Survey Water-Resources Investigations Report 01-4223.

Ellison, W. J., K. Lamkaouchi, and J. M. Moreau, 1996, Water: A dielectric reference: Journal of Molecular Liquids, **68**, 171–279.

Fuchs, M., M. J. Beres, and F. S. Anselmetti, 2004, Sedimentological studies of western Swiss lakes with high-resolution reflection seismic and amphibious GPR profiling: Proceedings of the 10th International Conference on Ground Penetrating Radar.

Haeni, F. P., M. L. Buursink, J. E. Costa, N. B. Melcher, R. T. Cheng, and W. J. Plant, 2000, Ground-penetrating RADAR methods used in surface-water discharge measurements: Proceedings of the 8th International Conference on Ground Penetrating Radar.

Hunter, L. E., M. G. Ferrick, and C. M. Collins, 2003, Monitoring sediment infilling at the Ship Creek Reservoir, Fort Richardson, Alaska, using GPR, *in* C. S. Bristow, and H. M. Jol, eds., Ground penetrating radar in sediments: Geological Society (of London) Special Publication, 211, 199–206.

Jol, H. M., and A. Albrecht, 2004, Searching for submerged lumber with ground penetrating radar: Rib Lake: Proceedings of the 10th International Conference on Ground Penetrating Radar.

Kingsley, S., and S. Quegan, 1992, Understanding radar systems: McGraw-Hill Book Company.

Kovacs, A., 1978, Remote detection of water under ice-covered lakes on the North Slope of Alaska: Arctic, **31**, 448–458.

Melcher, N. B., J. E. Costa, F. P. Haeni, R. T. Cheng, E. M. Thurman, M. Buursink, K. R. Spicer, E. Hayes, W. J. Plant, W. C. Keller, and K. Hayes, 2002, River discharge measurements by using helicopter-mounted radar: Geophysical Research Letters, **29**, 41-1–41-4.

Mellett, J. S., 1995, Profiling of ponds and bogs using ground-penetrating radar: Journal of Paleolimnology, **14**, 233–240.

Meyers, R. A., and D. G. Smith, 1998, Development of an underwater ground penetrating radar system: Proceedings of the 7th International Conference on Ground Penetrating Radar.

Moorman, B. J., W. M. Last, and J. P. Smol, 2001, Ground-penetrating radar applications in paleolimnology, *in* W. M. Last, and J. P. Smol, eds., Tracking environmental change using lake sediments: Physical and chemical techniques: Kluwer Academic Publishers, 23–47.

Moorman, B. J., and F. A. Michel, 1997, Bathymetric mapping and sub-bottom profiling through lake ice with ground-penetrating radar: Journal of Paleolimnology, **18**, 61–73.

Olimpio, J. R., 2000, Use of a ground-penetrating radar system to detect pre and post-flood scour at selected bridge sites in New Hampshire, 1996–98: U. S. Geological Survey Water-Resources Investigations Report 00-4035.

Park, I., J. Lee, and W. Cho, 2004, Assessment of bridge scour and riverbed variation by a ground penetrating radar: Proceedings of the 10th International Conference on Ground Penetrating Radar.

Porsani, J. L., L. Moutinho, and M. L. Assine, 2004, GPR survey in the Taquari River, Pantanal wetland, west-central Brazil: Proceedings of the 10th International Conference on Ground Penetrating Radar.

Powers, C. J., F. P. Haeni, and S. Spence, 1999, Integrated use of continuous seismic-reflection profiling and ground-penetrating radar methods at John's Pond, Cape Cod, Massachusetts: Proceedings of the Symposium on the Application of Geophysics to Engineering and Environmental Problems (SAGEEP), doi: 10.2113/1.2922628.

Sambuelli, L., S. Leggieri, C. Calzoni, and C. Porporato, 2007, Study of riverine deposits using electromagnetic methods at a low induction number: Geophysics, **72**, no. 5, B113–B120.

Schwamborn, G. J., J. K. Dix, J. M. Bull, and V. Rachold, 2002, High-resolution seismic and ground penetrating radar-geophysical profiling of a thermokarst lake in the western Lena delta, northern Siberia: Permafrost and Periglacial Processes, **13**, 259–269.

Sellmann, P. V., A. J. Delaney, and S. A. Arcone, 1992, Sub-bottom surveying in lakes with ground penetrating radar: U. S. Army Cold Regions Research and Engineering Laboratory report 92-8.

Shields, G., S. Grossman, M. Lockheed, and A. Humphrey, 2004, Waterborne geophysical surveys on shallow river impoundments: Proceedings of the Symposium on the Application of Geophysics to Engineering and Environmental Problems (SAGEEP), doi: 10.2113/1.2923266.

Sihvola, A. H., and E. Alanen, 1991, Studies of mixing formulae in the complex plane: IEEE Transactions on Geoscience and Remote Sensing, **29**, 679–687.

Tóth, T., 2004, High resolution geophysics provides optimal results on inland waterways: First Break, **22**, 45–51.

Ulriksen, C. P. F., 1982, Application of impulse radar to civil engineering: Ph.D. dissertation, Lund University of Technology.

Webb, D. J., N. L. Anderson, T. Newton, and S. Cardimona, 2000, Bridge scour: Application of ground penetrating radar: Proceedings of the First International Conference on the Application of Geophysical Methodologies and NDT to Transportation Facilities and Infrastructure, Federal Highway Commission and Missouri Department of Transportation, http://utc.mst.edu/pubs/conf/2000.html, accessed 23 March 2009.